

# Probing physical properties of confined fluids within individual nanobubbles

D. Taverna,<sup>1</sup> M. Kociak,<sup>1</sup> O. Stéphan,<sup>1</sup> C. Colliex,<sup>1</sup> A. Fabre,<sup>2</sup> E. Finot,<sup>3</sup> B. Décamps,<sup>4</sup> and C. Colliex<sup>1</sup>

<sup>1</sup>Laboratoire de Physique Solides, CNRS, UMR8502, Université Paris-Sud, Orsay, France

<sup>2</sup>C.E.A. Centre d' Etudes de Valduc, Is-sur-Tille, France

<sup>3</sup> Laboratoire de Physique, UMR CNRS 5027, Université de Bourgogne, Dijon, France

<sup>4</sup>Laboratoire de Chimie Métallurgique des Terres Rares, UPR 209 du CNRS, Thiais, France

(Dated: November 16, 2018)

Spatially resolved electron energy-loss spectroscopy (EELS) in a scanning transmission electron microscope (STEM) has been used to investigate as fluidic phase in nanobubbles embedded in a metallic  $Pd_{90}Pt_{10}$  matrix. Using the  $1s \rightarrow 2p$  excitation of the He atoms, maps of the He distribution, in particular of its density and pressure in bubbles of different diameter have been realized, thus providing an indication of the involved bubble formation mechanism. However, the short-range Pauli repulsion mechanism between electrons on neighboring atoms seems insufficient to interpret minute variations of the local local measurements performed at the interface between the metal and the He bubble. Simulations relying on the continuum dielectric model have shown that these deviations could be interpreted as an interface polarization effect on the He atomic transition, which should be accounted for when measuring the densities within the smaller bubbles.

Confined fluids in nanosized volumes constitute challenging objects for both basic and technological aspects. The investigation of the structural features and dynamics of nanojets has given rise to spectacular experimental studies and theoretical simulations [1]. Another ideal system is represented by gas confined in nanocavities. It is the case of inert gas atoms coalescing as a fluid or a solid to fill nanocavities in metals, with spherical or faceted morphologies depending of the local pressure. In the case of Xe in Al, an interfacial ordering has been demonstrated by high resolution electron microscopy [2]. These small gas-filled cavities therefore behave as high-pressure cells, providing the boundary conditions for the evaluation of the physical properties of encapsulated gases. A most challenging problem is the evaluation of gas density and pressure in such cavities.

Among the possible systems, He nanobubbles in metals have attracted the attention of many researchers, because of their high technological interest in the aging of the mechanical properties of materials involved in nuclear reactors [3]. Measurements averaging the information over large populations of bubbles, the size distribution of which being controlled by TEM, have first been performed by NMR [4] and by a combination of optical absorption and electron energy-loss spectroscopy (EELS) [5]. The first of these studies has revealed a solid-fluid transition at 250K for bubble pressures ranging from 6 to 11 GPa (i.e. He atomic densities from about 100 to 200  $\text{nm}^{-3}$ ). The second study comparing UV absorption spectroscopy on a synchrotron and high energy resolution EELS without spatial resolution on He<sup>+</sup> implanted Al thin foils, have identified the blue shift of the He  $1s \rightarrow 2p$  transition (with respect to its value of 21.218 eV for the free atom) as a hint for evaluating the local pressure. Theoretically, Lucas *et al.* [6] have confirmed that this blue shift of the He K-line should be attributed to the short-range Pauli repulsion between the electrons

of neighboring He atoms. Consequently, this effect should increase linearly with the density of the He atoms in the high-pressure fluid phase likely to exist in these nanosized bubbles. Jäger *et al.* [7] have confirmed this linear relation between the measured energy shifts ( $\Delta E$ ) and the average bubble radii ( $r$ ), the larger shift corresponding to the higher He density and consequently to the smaller radii.

With the development of scanning transmission electron microscopy (STEM) techniques, capable of measuring spatially resolved EELS spectra for different positions of a sub-nm probe on the specimen, new possibilities were offered to perform analysis on individual nanobubbles [8]. The most comprehensive study up-to-date has been conducted by Walsh *et al.* [9], who proposed a procedure for estimating directly the helium density in a single nanobubble. However, this work did not take into account the influence of interface excitations on the estimation of the internal density. A more fundamental issue which has not been addressed in the case of helium bubbles is the potential occurrence of density inhomogeneities close to the surface, due to the interaction between the confined fluid and the matrix. The investigation of such effects requires a refined characterization at a sub-nanometer scale.

In this letter, we present a study of the physical parameters (density, pressure, energy of the He K-line) defining the state of He inside nanobubbles, by using spatially resolved EELS to map their variations at the nanometer scale. The variations between bubbles of different size are in agreement with the standard interpretation in the literature, while a refined description is required for the evolution of the He signal within an individual bubble. By using the continuum dielectric model, we show that the discrepancies can be explained invoking an effect of surface polarization at the interface between the He and the metallic surface. This leads to the necessity of a cor-

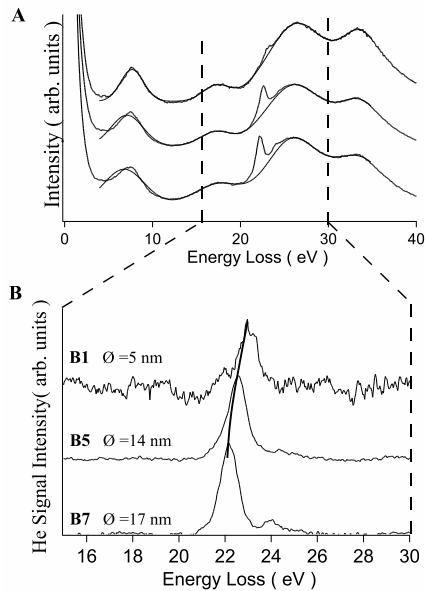


FIG. 1: **A:** EELS spectra acquired at the centre of bubbles of different size (thick lines) and corresponding fit of the Pd plasmon (thin lines). **B:** Subtracted He signal. The shift of the He K-line for bubbles of different size is obvious.

rection of the EELS estimation of the He density inside small bubbles.

The results are issued from an 8-month aged tritiated  $\text{Pd}_{90}\text{Pt}_{10}$  alloy which exhibits a largely dispersed population of voids (from 2 to 20 nanometers in diameter). The EELS measurements have been performed in a VG STEM HB 501 with a field emission gun operated at 100 kV and a homemade detection system formed by a Gatan 666 PEELS spectrometer optically coupled with a CCD camera. Spectrum-images made typically of  $64 \times 64$  spectra could then be acquired with the following conditions : acquisition time of 200 ms per spectrum, probe of 0.7 nm with step increments of ranging from 1.5 to 0.5 nm. Fig. 1A shows three EELS spectra corresponding to a selection of pixels at the centre of three bubbles of different sizes (B1, B5 and B7) visible on fig. 2A. These spectra correspond to positions where the electron beam has crossed both the metallic matrix and the bubbles. They all exhibit four major peaks (around 7, 17, 26 and 33 eV respectively), which are attributed to the low energy loss spectrum of the Pd alloy matrix. The sharper line between 22 and 23 eV is the signature of the He K edge.

In order to be more quantitative, the He signal of each spectrum has been isolated by fitting the palladium contribution with 4 Gaussian curves (fig. 1B). We can then identify any change in position, width, total intensity and possible occurrence of fine structures or satellites on the He K-line, related the different bubbles. For each probe position, the He K-line intensity can be evaluated by in-

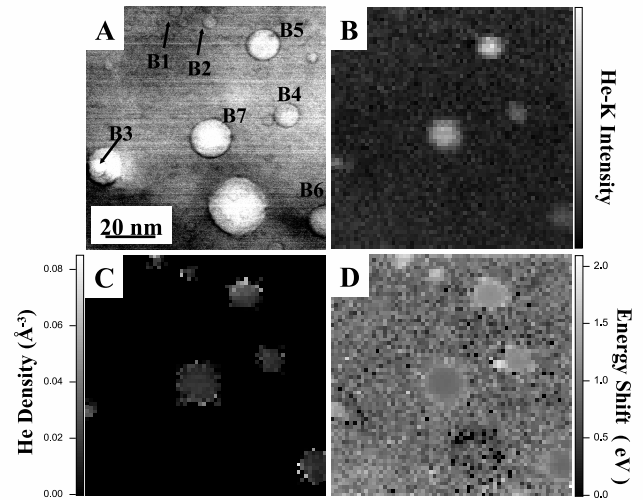


FIG. 2: Maps extracted from a spectrum-image of a selected area of the sample. **A:** Bright field image of the analyzed area. Bubbles showing He signal are evidenced. **B:** Helium chemical map. **C:** Map of the He density inside the He filled bubbles. **D:** Map of the energy shift of the He K-line. The reference energy is chosen as that of the atomic He (21.218 eV)

tegrating the signal over a window of typically 4 eV and the results ( $I_{He}$ ) are displayed as a 2D map (fig. 2B) of the localization of He atoms. It must be noticed that not all the voids contain He atoms. The next step is to transform the He K-line intensity map into a cartography of the absolute estimated He density  $n$  (expressed in atoms/ $\text{nm}^3$ ). This can be calculated from the relation [9]:  $n = I_{He} / (\sigma_{He} I_z d)$ , where  $\sigma_{He}$  is the cross section of the helium  $1s \rightarrow 2p$  transition for the used experimental conditions (see[9] for calculation),  $I_z$  is the integrated intensity of the elastic peak,  $d$  is the local thickness at the pixel position of the analyzed He nano-volume. This parameter is the source of highest uncertainties. We have tested several approaches, but finally we estimated it experimentally as the complement to local thickness measurements of the matrix. The resulting density map is shown on fig. 2C.

The mean helium density inside a bubble is estimated by averaging the calculated values over a selection of pixels corresponding to central positions. The results range from 15 to 35 He atoms per  $\text{nm}^3$ , the highest value been obtained for one of the smaller bubble B1. The energy shift, defined as the difference between the measured peak position inside the bubbles and the nominal K-line of atomic He [6], is mapped on fig. 2D and varies from about 1 up to 2 eV. In order to verify the predicted linear dependence of  $\Delta E(n)$ , we have plotted in fig. 3A our results issued from several spectrum-images (empty squares). A satisfactory fit to a law  $\Delta E = C_n n + D$  can be obtained with  $C_n = (44 \pm 7) \cdot 10^{-3} \text{eV} \cdot \text{nm}^3$  and  $D$

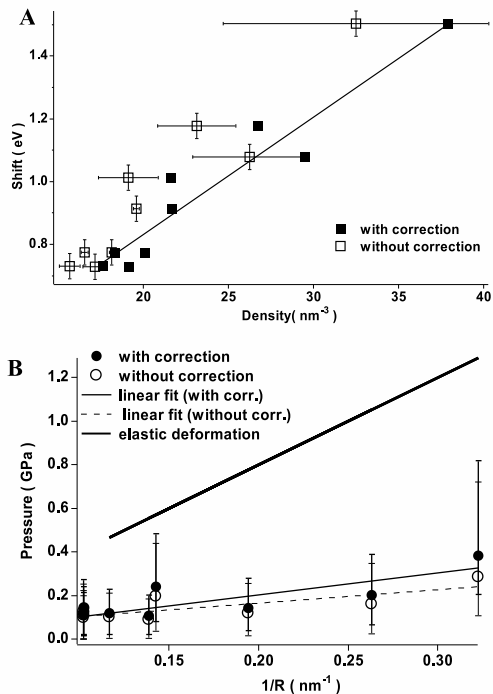


FIG. 3: **A:** Experimental relation between energy shift and measured density. Empty squares represent uncorrected density value; linear fit law:  $\Delta E = (0.044 \pm 0.007)n + (0.07 \pm 0.18)$ . Filled square represent density value corrected by surface effects; linear fit law:  $\Delta E = (0.037 \pm 0.004)n + (0.08 \pm 0.10)$ . Error bars correspond the standard deviation calculated on the selection of pixels of the density map, and therefore are large for small bubbles having a bad statistics. **B:** Experimental relation between pressure and the inverse of the bubble radius. Empty circles are deduced from uncorrected density values; linear fit law  $P = (0.6 \pm 0.2) \times 1/R + (0.04 \pm 0.05)$ . Filled circles account for surface effects; linear fit law  $P = (1.0 \pm 0.4) \times 1/R + (0.002 \pm 0.083)$ . The theoretical linear relation for elastic deformation of the Pd<sub>90</sub>Pt<sub>10</sub> matrix is also displayed. Error bars are estimated by calculating the variation of the equation of state in the density range defined by the corresponding density error bars. Error bars for corrected values (not shown) are identical to those for uncorrected values

$= 0.07 \pm 0.18 \text{ eV}$ . The value of  $C_n$  lies significantly higher than those measured by Jäger *et al.* [7] and Walsh *et al.* [9] but is close to that determined by McGibbon [8].

Another relevant parameter is the internal pressure. In fact, if the bubble deforms the matrix elastically, the radius dependence of the bubble pressure is supposed to obey an inverse proportionality law  $P = 2\gamma/r$  (where  $\gamma$  is the surface energy). Following the procedure indicated in [9], we calculate the pressure from the measured  $n$  by using a semi-empirical equation of states (see supplementary materials and [9, 10]). The results are shown in fig. 3B (empty circles). The pressure inside the bubbles is shown to increase roughly from 0.1 to 0.3 GPa (i.e. in a range well below the solid to liquid transition pressure),

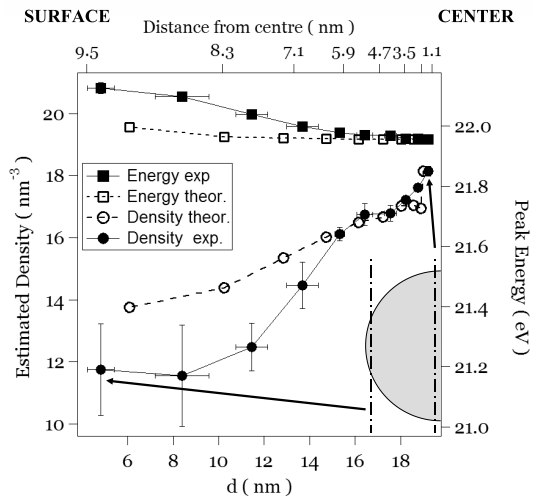


FIG. 4: Experimental profiles of the estimated density ( filled circles) and of the blue-shift of the He K-line (filled squares) as a function of the mean local thickness  $d$ . Data are extracted from a spectrum image of  $40 \times 40$  pixels (spatial sampling of 0.5 nm), acquired on a bubble of 19.5 nm diameter. For comparison, the corresponding simulated profiles of the He-K line density (empty circles) and energy position (empty square) are also displayed.

when the diameter of the bubble decreases from 17 to 5 nm. A reasonable value for the surface energy of the Pd<sub>90</sub>Pt<sub>10</sub> alloy is  $\gamma = 1.9 \text{ Jm}^{-2}$ , to be compared to our experimental slope  $0.3 \text{ Jm}^{-2}$ . Then, the bubbles seem to be under-pressured at the moment of our TEM observation.

The spectrum-image technique offers the extra possibility of exploring any potential intra-inclusion spatial dependence. A varying contrast seems visible within larger bubbles in fig. 2C and 2D, where the density drops while the energy shift increases close to the surface of the bubbles. In order to further investigate this behavior, fig. 4 shows experimental profiles of density and shift as elaborated from a spectrum-image of a 19.5 nm bubble, probed with a better lateral sampling of 0.5 nm. Each point of the two profiles has been calculated selecting annular regions of pixels corresponding to the same analyzed thickness, and fitting the He  $1s \rightarrow 2p$  transition with a Gauss function to calculate the energy position and the intensity. From the centre to the bubble surface a 37 percent drop is observed for  $n$  while the energy shift increases by 0.17 eV, which is one order of magnitude smaller than the shift between different bubbles. This anticorrelation is in contradiction with the general tendency previously observed between individual bubbles. Indeed, when only Pauli repulsion between He atoms is taken into account, such a density drop should lead to a 0.35 eV shift toward *lower* energies. In order to evaluate the potential occurrence of surface effects, we have performed EELS spectra simulations, by adapting

to the case of embedded spheres the continuum dielectric model which has proved its efficiency for modeling local surface phenomena in nanosized systems, such as single-walled nanotubes [11, 12]. As an input for the simulation, we used a lorentzian dielectric constant corresponding to a He fluid of *constant* density [6]. After simulation of spectra for different local thicknesses  $d$ , the procedure used to extract  $n$  and  $\Delta E$  on experimental data is applied. The resulting simulated profiles are compared to the experimental ones in fig. 4B. Both  $\Delta E$  and  $n$  variations are reproduced but underestimated. Consequently, the major part of the effect can not be attributed to a real change in the density, since the model assumes a constant one, but to the influence of surface excitations on the measurement. We stress that the evidenced surface effect is not due to an usual plasmon mode, because it does not correspond to a pole (resonance) but to a maximum of the dielectric response of the sphere  $Im((\epsilon_{He}-\epsilon_m)/(\epsilon_{He}+2\epsilon_m))$  (where  $\epsilon_{He}$  and  $\epsilon_m$  are the dielectric constants of He and of the metallic matrix respectively). An interface plasmon excitation is expected at a lower energy value (of the order of 7 eV), and is rather insensitive to the helium density. However, the dielectric formalism commonly used to model plasmon excitations furnishes reliable (similar) interpretations for the effects of interface polarization on the atomic transition. It is well known that such a formalism is very sensitive to the input dielectric constants of both materials, and discrepancies between simulated and experimental data can be partially explained by a lack accuracy of the lorentzian model adopted for He as well as of the experimental data used for Pd. Nevertheless, the energy shift of He K-line is explained by the contribution of a surface “mode” which energy, for this particular system, is slightly higher than that of the bulk He line (see supplementary materials). The decrease of the estimated density can be related to a companion effect known, for plasmons, as a boundary effect or “Begrenzung” effect [13]. This effect is commonly interpreted as a modification in the probability to excite bulk modes due to the occurrence of surface excitation, and reveals itself as a negative contribution to the intensity of the bulk He line, the importance of which increases as the He thickness decreases. We point out that this is the first time that this surface effect, which has been thoroughly investigated for valence electron excitations, is evidenced on an atomic-type excitation, using EELS.

Therefore, beside its intrinsic fundamental interest, this surface-induced decrease in the density estimated from atomic transition signal should be taken into account in the study of the bubble formation mechanism. We calculated a correction coefficient  $G$  to apply to experimental intensities in order to account for surface effects in the estimation of  $n$ . Such a coefficient is given by the ratio  $G = I_{wos}/I_{tot}$ , where  $I_{wos}$  is the He-K intensity simulated excluding surface contributions (ideal

case), and  $I_{tot}$  is the total simulated intensity (real case). The resulting  $\Delta E(n)$  corrected relation is displayed in fig. 3A (filled squares). The linear fit gives an estimation of the slope  $C_n$  decreased of 19 percent and closer to the values in the literature. Even larger is the correction to relation between the pressure and the inverse radius (filled circles in fig. 3B), with a slope increased by a factor close to 2. Nevertheless the comparison of the corrected data-set to the linear relation characteristic of the elastic deformation regime (also displayed in 3B) confirms that the bubbles are under pressured.

In conclusion, the present analysis of the confined He fluidic phase, at their interface with the embedding material, has evidenced an interface-induced effect on the atomic-like spectral transition in He. Consequently, a reliable estimation of the helium internal density and pressure requires a correction from this surface effect, especially in the case of small bubbles. This effect can be of much broader interest, and it should also be identified in quite different situations, such as those encountered on semi-core loss edges (Hf- $O_{2,3}$ ) in dielectric thin films [14]. From another point of view, the interpretation of residual discrepancies between experiments and simulations, when exploring the influence of the distance from the interface, require further modeling, accounting for changes in Pauli repulsion and in Van der Waals forces close to the interfaces.

We thanks L. Henrard, A. A. Lucas, Ph. Lambin and P. Loubeyre for fruitful discussions

- 
- [1] M. Moseler and U. Landman, *Science* **289**, 1165 (2000).
  - [2] S. Donnelly, R. Birtcher, C. Allen, I. Morrison, K. Furuya, M. Song, K. Mitsuishi, and U. Dahmen, *Science* **296**, 507 (2002).
  - [3] A. A. Lucas, *Physica B* **127**, 225 (1984).
  - [4] G. Abell and A. Attalia, *Phys. Rev. Lett.* **59**, 995?997 (1987).
  - [5] J. Rife, S. Donnelly, A. Lucas, J. Gilles, and J. Ritsko, *Phys. Rev. Lett.* **46**, 1220 (1981).
  - [6] A. Lucas, J. Vigneron, S. Donnelly, and J. Rife, *Phys. Rev. B* **28**, 2485 (1983).
  - [7] W. Jäger, R. Manzke, H. Trinkaus, R. Zeller, J. Fink, and G. Creelius, *Radiation Effects* **78**, 315 (1983).
  - [8] A. McGibbon, *Inst. Phys. Conf. Ser.* **119**, 109 (1991).
  - [9] C. Walsh, J. Yuan, and L. Brown, *Phil. Mag. A* **80**, 1507 (2000).
  - [10] H. Trinkhaus, *Radiation Effects* **78**, 189 (1983).
  - [11] O. Stéphan, D. Taverna, M. Kociak, K. Suenaga, L. Henrard, and C. Colliex, *Phys. Rev. B* **66**, 155422 (2002).
  - [12] D. Taverna, M. Kociak, V. Charbois, L. Henrard, O. Stéphan, and C. Colliex, *J. Electron Spectroscopy and Related Phenomena* **129**, 293 (2003).
  - [13] J. Geiger and K. Wittmaack, *Z. Physik* **195**, 44 (1966).
  - [14] M. Couillard, M. Kociak, O. Stéphan, G. A. Botton, and C. Colliex, submitted (2007).